Journal of Power Sources 196 (2011) 7715–7720

Contents lists available at ScienceDirect

Journal of Power Sources

journal homepage: www.elsevier.com/locate/jpowsour

Synthesis and improved electrochemical performances of porous $Li_3V_2(PO_4)_3$/C spheres as cathode material for lithium-ion batteries

Y.Q. Qiao, J.P. Tu*, X.L. Wang, D. Zhang, J.Y. Xiang, Y.J. Mai, C.D. Gu

State Key Laboratory of Silicon Materials and Department of Materials Science and Engineering, Zhejiang University, Hangzhou 310027, China

ARTICLE INFO

Article history:
Received 30 January 2011
Received in revised form 7 April 2011
Accepted 27 April 2011
Available online 4 May 2011

Keywords:
Lithium vanadium phosphate
Porous sphere
Hydrazine hydrate
Lithium ion battery

ABSTRACT

Spherical $Li_3V_2(PO_4)_3$/C composites are synthesized by a soft chemistry route using hydrazine hydrate as the spheroidizing medium. The electrochemical properties of the materials are investigated by galvanostatic charge–discharge tests, cyclic voltammograms and electrochemical impedance spectrum. The porous $Li_3V_2(PO_4)_3$/C spheres exhibit better electrochemical performances than the solid ones. The spherical porous $Li_3V_2(PO_4)_3$/C electrode shows a high discharge capacity of 129.1 and 125.6 mAh g^{-1} between 3.0 and 4.3 V, and 183.8 and 160.9 mAh g^{-1} between 3.0 and 4.8 V at 0.2 and 1 C, respectively. Even at a charge–discharge rate of 15 C, this material can still deliver a discharge capacity of 100.5 and 121.5 mAh g^{-1} in the potential regions of 3.0–4.3 V and 3.0–4.8 V, respectively. The excellent electrochemical performance can be attributed to the porous structure, which can make the lithium ion diffusion and electron transfer more easily across the $Li_3V_2(PO_4)_3$/electrolyte interfaces, thus resulting in enhanced electrode reaction kinetics and improved electrochemical performance.

1. Introduction

Monoclinic $Li_3V_2(PO_4)_3$ has attracted extensive interest as a potential cathode material for lithium-ion batteries due to its good ion mobility, high theoretical capacity (197 mAh g^{-1}) and high operating voltage [1,2]. $Li_3V_2(PO_4)_3$ possesses a NASICON-type structure consisting of slightly distorted VO_6 octahedra and PO_4 tetrahedra that share oxygen vertices with mobile Li^+ ions housed within the framework [1,3,4]. This NASICON-type structure with relatively larger interstitial space created by the PO_4^{3-} units is in favor of the fast ionic conductivity [5–8]. However, $Li_3V_2(PO_4)_3$ as well as $LiFePO_4$ have a problem of low intrinsic electronic conductivity (2.4×10^{-7} S cm^{-1}) [9], which greatly impedes their practical application. To solve this problem, various methods have been employed to overcome this disadvantage, such as doping with foreign atoms [10–14], decreasing the particle size [5,15] and carbon coating [16–27].

As has been reported in previous publication [15], nanosized $Li_3V_2(PO_4)_3$ favors excellent electrochemical performance due to the enhanced specific surface area and reduced diffusion length of the ions and electrons in the electrode. However, the nanosized particles are unfavorable for electrode preparation because they have very high specific surface area and high surface energy [28–30]. Further, nanosized particles have the drawback of electrochemical agglomeration during electrochemical cycling [28]. It has been reported [28–36] that the spherical morphology has many advantages in comparison with irregular aggregation such as higher volumetric energy density, lower interfacial energy, higher tap density and better fluidity characteristics. Traditionally, spray drying method is one of the most widely used techniques for preparation of spherical materials such as in the case of $LiMn_2O_4$ [37] and $LiFePO_4$ [29,30,38,39]. Recently, Wang et al. [40] successfully synthesized spherical $Li_3V_2(PO_4)_3$ by using N_2H_4 as reducer and the material exhibited initial discharge capacities of 123 mAh g^{-1} (0.2 C) and 132 mAh g^{-1} (0.5 C) in the potential ranges of 3.0–4.3 V and 3.0–4.8 V, respectively.

In the present work, we present a soft chemistry route to obtain spherical $Li_3V_2(PO_4)_3$/C by using hydrazine hydrate as the spheroidizing medium. Hydrazine hydrate was also acting as a reducer to reduce partially V^{5+} to lower valence at room temperature and then carbothermal reduction method was performed at high temperature to obtain the spherical $Li_3V_2(PO_4)_3$/C. Herein, porous $Li_3V_2(PO_4)_3$/C spheres can be obtained by adjusting the pH value of the solution. Porous spherical particles show great advantages such as good contact with electrolyte, high specific surface area, quick Li^+ permeation and easier to bind than isolated nanosized particles [29,30,38,39]. Therefore, we prepared two types of spherical $Li_3V_2(PO_4)_3$/C composites with porous and solid structures and their electrochemical performances were investigated.

* Corresponding author. Tel.: +86 571 87952856; fax: +86 571 87952573.
E-mail address: tujp@zju.edu.cn (J.P. Tu).

0378-7753/$ – see front matter © 2011 Elsevier B.V. All rights reserved.
doi:10.1016/j.jpowsour.2011.04.057

2. Experimental

The spherical $Li_3V_2(PO_4)_3$/C composites were synthesized using a soft chemistry route followed by a carbothermal reduction synthesis. Here, hydrazine hydrate was used as the spheroidizing medium and 1,4-dihydroxy-2-butyne was employed as the carbon source. First, NH_4VO_3 (5 g) was added to 20 mL of deionized water under magnetic stirring to obtain a white turbid liquid. Then stoichiometric of 30 mL $LiOH{\cdot}H_2O$ (2.83 g) solution was added to the above white turbid liquid under magnetic stirring at room temperature until a transparent solution was formed. An appropriate quantity of hydrazine hydrate was added dropwise to this transparent solution under magnetic stirring until the solution was become to straw yellow. Afterward, 30 mL of $(NH_4)_2HPO_4$ (8.465 g) solution and 30 mL of 1,4-dihydroxy-2-butyne (2 g) solution were added to the straw yellow solution gradually. The resulting solution with a pH value of 9.0–10.0 was transferred into a polytetrafluoroethylene (PTFE) container and sealed at 200 °C for 12 h, and then cooled to room temperature. Finally, the resulting precursor was washed with deionized water, separated by centrifugation for several times and dried at 60 °C (denoted as precursor-1). The processing conditions of the precursor of porous $Li_3V_2(PO_4)_3$/C spheres (denoted as precursor-2) were the same as those of the precursor-1 except the pH value of the solution was adjusted at 13.0–14.0 by adding appropriate of ammonia before transferred into the PTFE container. The two precursors were sintered at 750 °C for 10 h under Ar flow in a tube furnace to obtain the spherical $Li_3V_2(PO_4)_3$/C powders. The final product obtained from precursor-1 was solid sphere (denoted as SS-LVP/C), while the product obtained from precursor-2 was porous sphere (denoted as PS-LVP/C).

The morphologies and structures of the as-synthesized powders were characterized using field emission scanning electron microscopy (FESEM, FEI SIRION) and X-ray diffraction (XRD, Philips PC-APD with Cu Kα radiation). The residual carbon contents of the powders were determined by means of an automatic elemental analyzer (EA, Flash EA1112). Raman scattering spectroscopy (LABRAM HR-800) was recorded at room temperature with the wave number shift among 4000–100 cm^{-1} in ultraviolet laser excitation line of 325 nm.

Electrochemical performances of the spherical $Li_3V_2(PO_4)_3$/C composites were investigated using CR2025 coin-type cell. A metallic lithium foil served as the anode electrode. The cathode consisted of 85 wt.% active material, 10 wt.% acetylene black and 5 wt.% polyvinylidene fluoride (PVDF) on aluminum foil. 1 M $LiPF_6$ in ethylene carbonate (EC)–dimethyl carbonate (DMC) (1:1 in volume) as the electrolyte, and a polypropylene micro-porous film (Celgard 2300) as the separator. The cells were assembled in a glove box filled with high-purity argon. The charge–discharge tests were conducted on LAND battery program-control test system (Wuhan, China) between 3.0 and 4.3 V, 3.0 and 4.8 V by applying from 0.1 to 15 C current densities at room temperature, respectively. For electrochemical impedance spectroscopy (EIS) measurements, the test cells were with the metallic lithium foil as both the reference and counter electrodes. EIS measurements were performed on CHI660C electrochemical workstation over a frequency range of 100 kHz to 10 mHz at a stage of discharge (3.0 V) by applying an AC signal of 5 mV. Cyclic voltammetry (CV) was performed on this electrochemical workstation in the potential ranges of 3.0–4.3 V and 3.0–4.8 V (vs. Li/Li^+) at a scan rate of 0.1 mV s^{-1}, respectively.

3. Results and discussion

Fig. 1 shows the XRD patterns of SS-LVP/C and PS-LVP/C composites. The diffraction peaks of both samples can be attributed to monoclinic $Li_3V_2(PO_4)_3$ with the space group of $P2_1/n$ (ICSD

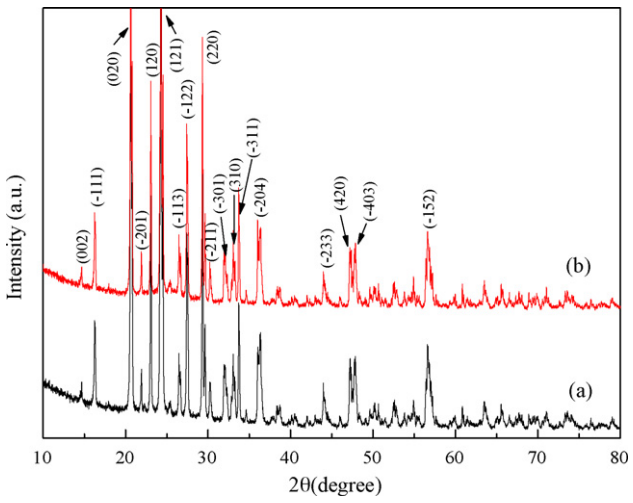

Fig. 1. XRD patterns of (a) SS-LVP/C and (b) PS-LVP/C composites.

#96962). Although about 11 wt.% 1,4-dihydroxy-2-butyne (carbon source) of total weight of the raw materials is used for the preparation of $Li_3V_2(PO_4)_3$/C composites, the residual carbon is not detected in the XRD patterns since the state of the carbon is amorphous, or the amount of carbon is too small to be detected. However, according to elemental analysis, the carbon content in the final products is 2.87 and 2.62 wt.% for the SS-LVP/C and PS-LVP/C samples, respectively. Raman scattering results also indicate the presence of residual carbon in the $Li_3V_2(PO_4)_3$/C composites, as shown in Fig. 2. In the two Raman spectra, two intense broad bands at 1590 cm^{-1} and 1353 cm^{-1} are attributed to the graphite band (G-band) and the disorder-induced phonon mode (D-band), respectively. According to the fitting results, the I_D/I_G value of the SS-LVP/C and PS-LVP/C composite is 0.88 and 0.87, respectively. This suggests that the graphite-like carbon in the residual carbon is about 50%, which is similar to the previous reports [7,18]. It is believed that low ratio value (I_D/I_G) of carbon coating is helpful for improving the electronic conductivity and electrochemical performance of $Li_3V_2(PO_4)_3$ [7,18]. In addition, there are three broad Raman bands at 1136, 1050 and 970 cm^{-1}, which can be assigned to the vibrations of $Li_3V_2(PO_4)_3$ [41].

Fig. 3 shows the SEM images of precursors and spherical $Li_3V_2(PO_4)_3$/C powders. As seen in Fig. 3a, precursor-1 has a spherical morphology but with a non-uniform size distribution. The

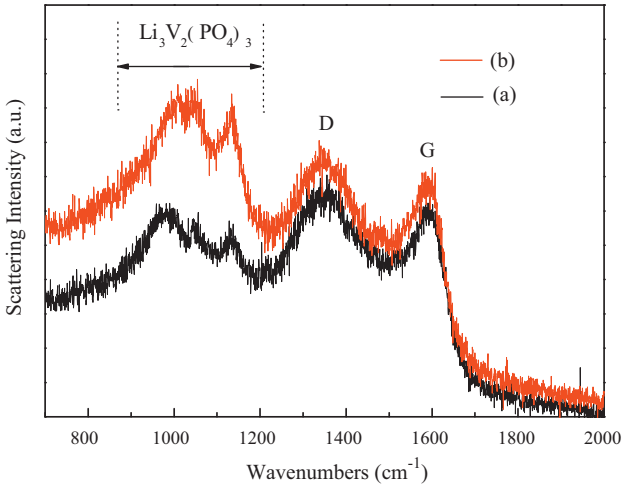

Fig. 2. Raman scattering spectra of (a) SS-LVP/C and (b) PS-LVP/C composites.

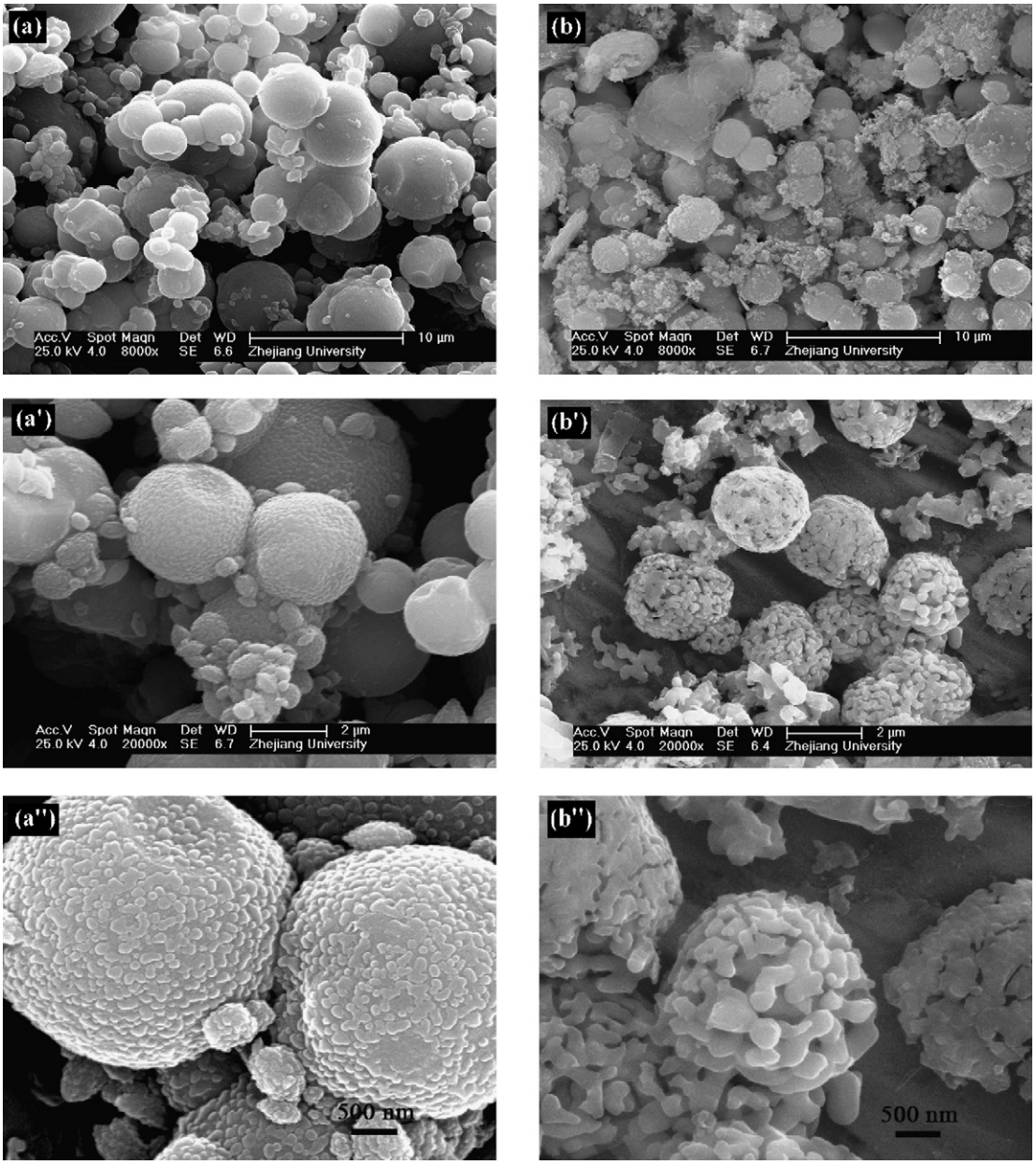

Fig. 3. SEM images of precursors and spherical $Li_3V_2(PO_4)_3$/C composites: (a) precursor-1, (a′) SS-LVP/C and (a″) magnified image of SS-LVP/C; (b) precursor-2, (b′) PS-LVP/C and (b″) magnified image of PS-LVP/C.

observed spheres are 0.5–7 μm in sizes. In Fig. 3b, precursor-2 also shows spherical morphology but with a relatively good uniformity of 2–5 μm in sizes. It is also found that the surface of precursor-1 is more smooth and denser than that of precursor-2. It is clearly seen that the pH value has an obvious influence on the morphologies of the precursors, which may have significant impact on the characteristics of the final products. After the heat treatment at 750 °C for 10 h, both of the samples remain spherical morphologies. For SS-LVP/C, the spheres are solid (Fig. 3a′ and a″). In contrast to SS-LVP/C, the PS-LVP/C particles contain a large number of internal pores (Fig. 3b′ and b″). Large solid aggregates of the as-synthesized SS-LVP/C powder would seriously impede its electrochemical performance. However, the porous structure can promote good electrical contact among the $Li_3V_2(PO_4)_3$ particles and help the electrolyte to penetrate the material, thus highly favors the solid-state diffusion kinetics and improves the capacity of the electrode material [29,30,42].

Fig. 4 shows initial charge–discharge curves of the SS-LVP/C and PS-LVP/C composites in the potential ranges of 3.0–4.3 V and 3.0–4.8 V. Between 3.0 and 4.3 V, the cells exhibit three charge plateaus and correspondingly three discharge plateaus (Fig. 4a and b), which are identified as the two-phase transition processes during the electrochemical reactions [5]. Between 3.0 and 4.8 V, all three of the Li^+ ions can be extracted and four charge plateaus are found during the charge process (Fig. 4c and d), but the discharge process exhibits three discharge plateaus, which are similar to the previous reports [1,17,40]. However, with the increase of charge–discharge rate, these plateaus become shorter and the differences of the charge and discharge plateaus become larger gradually which can be attributed to the electrode polarization at high rates. It is clearly seen that the PS-LVP/C electrode presents higher discharge capacities than SS-LVP/C. For instance, the PS-LVP/C electrode can deliver a discharge capacity of 129.1, 125.6, 115.7 and 100.5 mAh g^{-1} between 3.0 and 4.3 V at 0.2, 1, 10 and

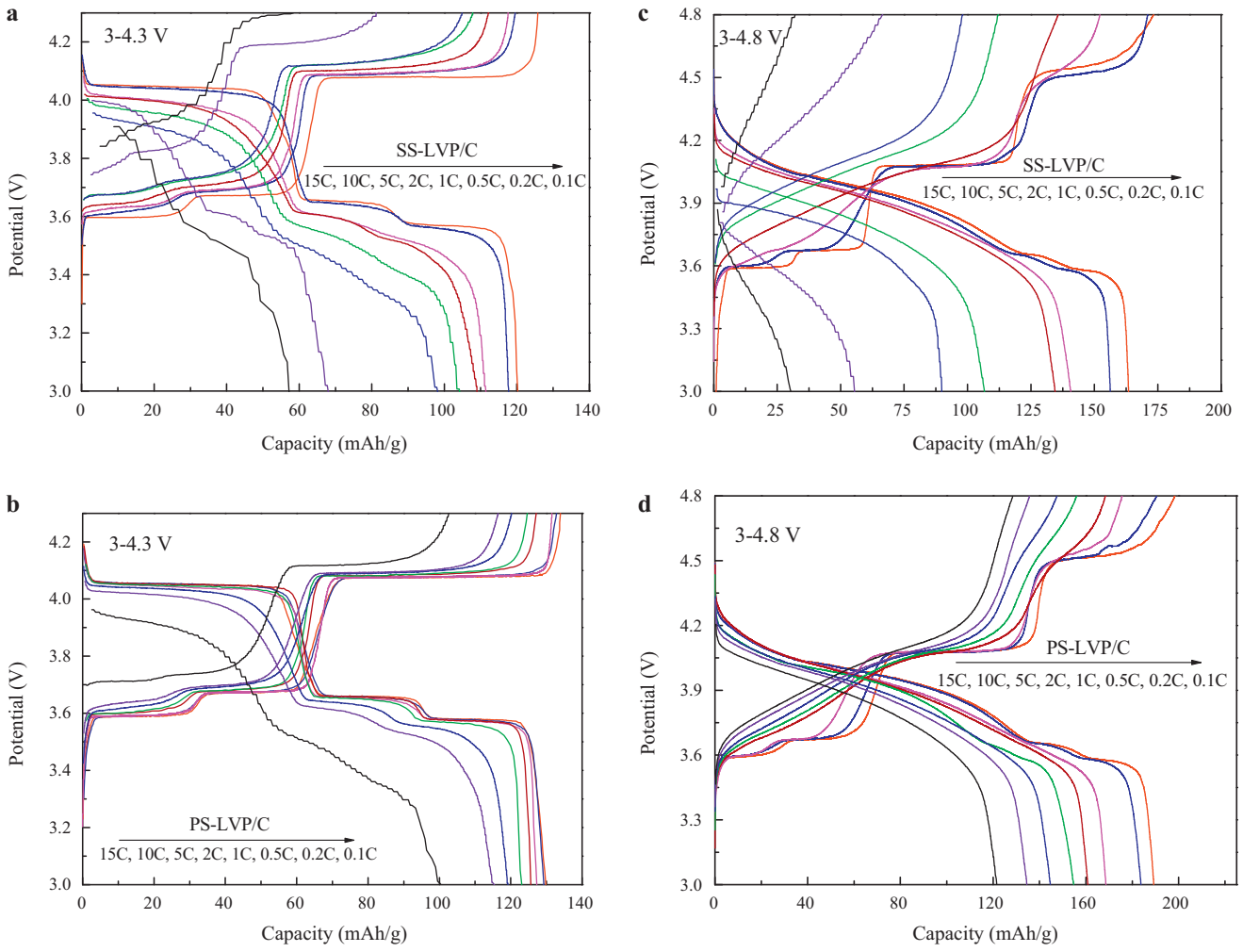

Fig. 4. Initial charge–discharge curves of spherical $Li_3V_2(PO_4)_3$/C composites in the potential ranges of 3.0–4.3 V and 3.0–4.8 V: (a) and (c) for SS-LVP/C; (b) and (d) for PS-LVP/C.

15 C rate, respectively, while the SS-LVP/C electrode is 117.7, 109, 68.3 and 57.7 mAh g^{-1}, respectively. Between 3.0 and 4.8 V, the discharge capacity of the PS-LVP/C electrode at 0.2, 1, 10 and 15 C rate is 183.8, 160.9, 134.5 and 121.5 mAh g^{-1}, respectively, whereas the SS-LVP/C electrode exhibits 156.3, 134.5, 55.5 and 30.7 mAh g^{-1}, respectively. Fig. 5 presents the rate capability of SS-LVP/C and PS-LVP/C composites in the potential ranges of 3.0–4.3 V and 3.0–4.8 V. It is also clearly seen that the PS-LVP/C electrode shows excellent rate capability. When the charge–discharge rate is decreased to 0.1 C, the discharge capacity of the PS-LVP/C electrode can still

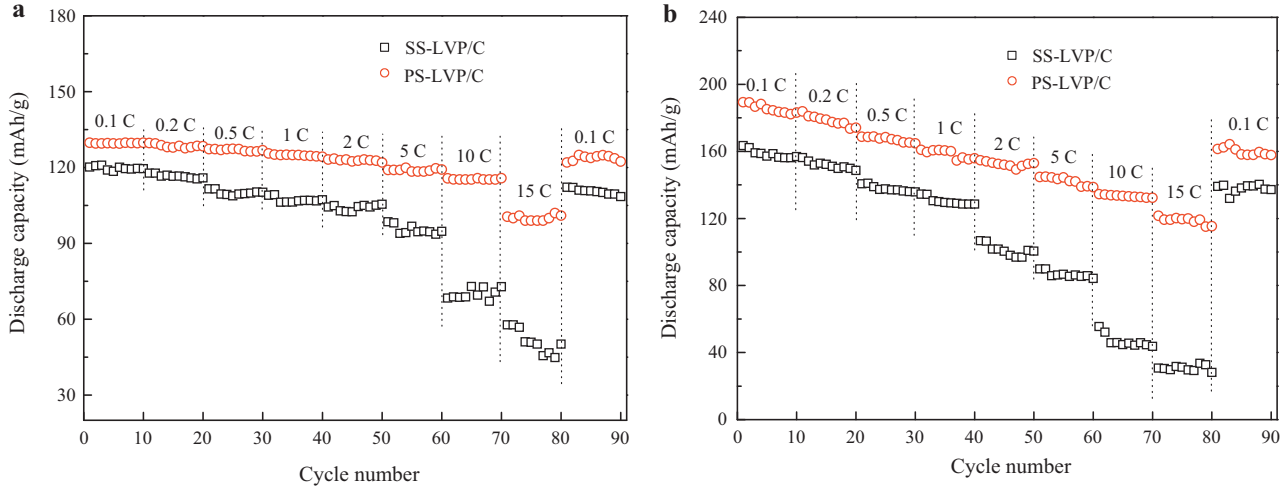

Fig. 5. Rate capability of SS-LVP/C and PS-LVP/C composites in the potential ranges: (a) 3.0–4.3 V and (b) 3.0–4.8 V.

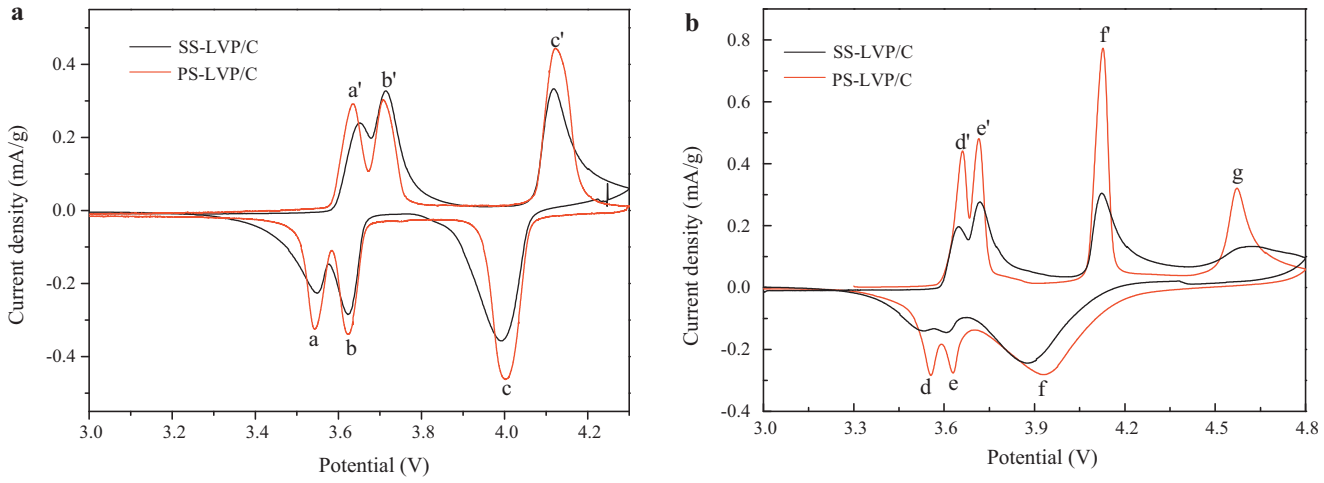

Fig. 6. CV curves of SS-LVP/C and PS-LVP/C composites in the potential ranges: (a) 3.0–4.3 V and (b) 3.0–4.8 V. Scan rate: 0.1 mV s^{-1}.

Table 1
Potential differences between the oxidation and reduction peaks for SS-LVP/C and PS-LVP/C electrodes (Fig. 6).

	$\Delta E_{a'-a}$ (V)	$\Delta E_{b'-b}$ (V)	$\Delta E_{c'-c}$ (V)	$\Delta E_{d'-d}$ (V)	$\Delta E_{e'-e}$ (V)	$\Delta E_{f'-f}$ (V)	ΔE_{g-f} (V)
SS-LVP/C	0.112	0.101	0.123	0.112	0.111	0.240	0.701
PS-LVP/C	0.100	0.092	0.121	0.101	0.090	0.189	0.641

reach 122.0 and 161.4 mAh g^{-1} in the potential ranges of 3.0–4.3 V and 3.0–4.8 V, respectively.

CV curves of SS-LVP/C and PS-LVP/C composites in the potential ranges of 3.0–4.3 V and 3.0–4.8 V are shown in Fig. 6. Both the electrodes present three couples of oxidation and reduction peaks between 3.0 and 4.3 V (Fig. 6a, labeled as a′/a, b′/b and c′/c), while in the potential range of 3.0–4.8 V, four oxidation peaks (labeled as d′, e′, f′ and g) and three reduction peaks (labeled as d, e and f) can be observed in the curves (Fig. 6b). These results are in good agreement with the charge–discharge plateaus presented in Fig. 4 and some previous publications [6,22]. Notably, the CV curves of PS-LVP/C composite exhibit more highly symmetrical and sharper anodic/cathodic peaks than the SS-LVP/C composite. Furthermore, as concluded in Table 1, the potential differences between anodic peaks and cathodic peaks are smaller in the PS-LVP/C electrode. It indicates the enhanced electrode reaction reversibility of PS-LVP/C electrode due to the porous structure. Therefore, the PS-LVP/C composite has higher discharge capacity and better cyclic ability.

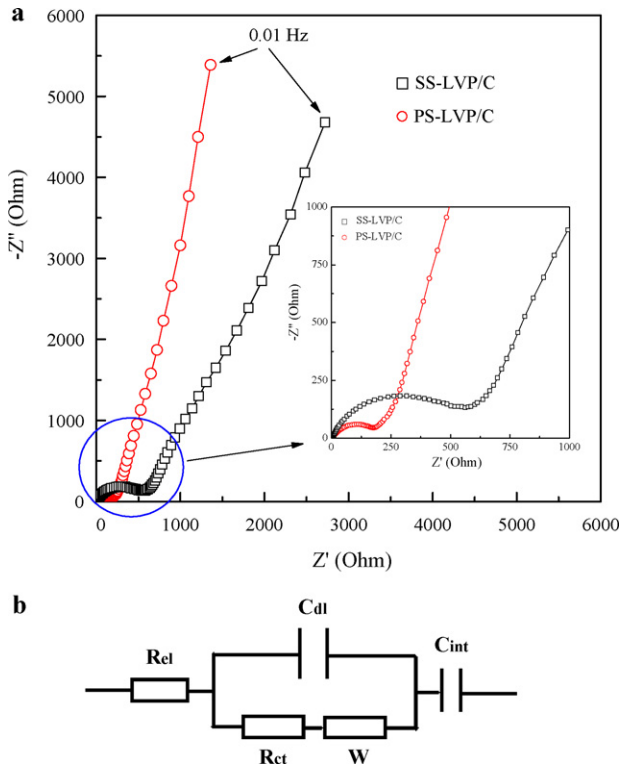

Fig. 7. (a) Nyquist plots for SS-LVP/C and PS-LVP/C composites at a stage of discharge (3.0 V). (b) Equivalent circuit used for simulating the experimental impedance data.

EIS measurements are carried out in the frequency range of 100 kHz to10 mHz at the discharge state (3.0 V) after 3 cycles, and the Nyquist plots of the $Li_3V_2(PO_4)_3$/C electrodes are shown in Fig. 7a. Fig. 7b presents an equivalent circuit to simulate the electrochemical impedance data. R_{el} represents the solution resistance; R_{ct} and C_{dl} stand for the related charge-transfer resistance and double-layer capacitance, respectively; W represents the diffusion-controlled Warburg impedance in the low frequency [11,43]. C_{int} stands for the Li^+ intercalation capacitance [11,44–46]. It is found that the R_{ct} value of PS-LVP/C electrode (117.1 Ω) is much smaller than that of SS-LVP/C (510.5 Ω), indicating that the electrons and Li ions can transfer more quickly due to the porous structure. Thus, the PS-LVP/C composite exhibits the enhanced electrode reaction kinetics and improved electrochemical performance.

4. Conclusions

Spherical $Li_3V_2(PO_4)_3$/C composites were successfully prepared by using hydrazine hydrate as the spheroidizing medium. Electrochemical tests show that the spherical $Li_3V_2(PO_4)_3$/C with pores exhibited excellent electrochemical performance. At a charge–discharge rate of 15 C, this composite could deliver a discharge capacity of 100.5 and 121.5 mAh g^{-1} in the potential regions of 3.0–4.3 V and 3.0–4.8 V, respectively. The excellent electrochemical performance should be attributed to the porous structure, which can make the lithium ion diffusion and electron transfer more easily across the $Li_3V_2(PO_4)_3$/electrolyte interfaces, thus resulting in the

enhanced electrode reaction kinetics and improved electrochemical performance.

References

[1] S.-C. Yin, H. Grondey, P. Strobel, H. Huang, L.F. Nazar, J. Am. Chem. Soc. 125 (2003) 326.
[2] H. Huang, T. Faulkner, J. Barker, M.Y. Saidi, J. Power Sources 189 (2009) 748.
[3] M.Y. Saïdi, J. Barker, H. Huang, J.L. Swoyer, G. Adamson, J. Power Sources 119–121 (2003) 266.
[4] X.H. Rui, N. Ding, J. Liu, C. Li, C.H. Chen, Electrochim. Acta 55 (2010) 2384.
[5] H. Huang, S.-C. Yin, T. Kerr, N. Taylor, L.F. Nazar, Adv. Mater. 14 (2002) 1525.
[6] Y.Z. Li, Z. Zhou, X.P. Gao, J. Yan, Electrochim. Acta 52 (2007) 4922.
[7] T. Jiang, W.C. Pan, J. Wang, X.F. Bie, F. Du, Y.J. Wei, C.Z. Wang, G. Chen, Electrochim. Acta 55 (2010) 3864.
[8] Y.Q. Qiao, X.L. Wang, Y. Zhou, J.Y. Xiang, D. Zhang, S.J. Shi, J.P. Tu, Electrochim. Acta 56 (2010) 510.
[9] S.-C. Yin, P.S. Strobel, H. Grondey, L.F. Nazar, Chem. Mater. 16 (2004) 1456.
[10] S.Q. Liu, S.C. Li, K.L. Huang, Z.H. Chen, Acta Phys. -Chim. Sin. 23 (2007) 537.
[11] J.S. Huang, L. Yang, K.Y. Liu, Y.F. Tang, J. Power Sources 195 (2010) 5013.
[12] C.S. Dai, Z.Y. Chen, H.Z. Jin, X.G. Hu, J. Power Sources 195 (2010) 5775.
[13] Q. Kuang, Y.M. Zhao, X.N. An, J.M. Liu, Y.Z. Dong, L. Chen, Electrochim. Acta 55 (2010) 1575.
[14] Y.H. Chen, Y.M. Zhao, X.N. An, J.M. Liu, Y.Z. Dong, L. Chen, Electrochim. Acta 54 (2009) 5844.
[15] A.Q. Pan, J. Liu, J.-G. Zhang, W. Xu, G.Z. Cao, Z.M. Nie, B.W. Arey, S.Q. Liang, Electrochem. Commun. 12 (2010) 1674.
[16] M.M. Ren, Z. Zhou, X.P. Gao, W.X. Peng, J.P. Wei, J. Phys. Chem. C 112 (2008) 5689.
[17] Y.Q. Qiao, X.L. Wang, J.Y. Xiang, D. Zhang, W.L. Liu, J.P. Tu, Electrochim. Acta 56 (2011) 2269.
[18] J.W. Wang, J. Liu, G.L. Yang, X.F. Zhang, X.D. Yan, X.M. Pan, R.S. Wang, Electrochim. Acta 54 (2009) 6451.
[19] X.H. Rui, C. Li, J. Liu, T. Cheng, C.H. Chen, Electrochim. Acta 55 (2010) 6761.
[20] J.W. Wang, X.F. Zhang, J. Liu, G.L. Yang, Y.C. Ge, Z.J. Yu, R.S. Wang, X.M. Pan, Electrochim. Acta 55 (2010) 6879.
[21] G. Yang, H.M. Ji, H.D. Liu, B. Qian, X.F. Jiang, Electrochim. Acta 55 (2010) 3669.
[22] L. Zhang, X.L. Wang, J.Y. Xiang, Y. Zhou, S.J. Shi, J.P. Tu, J. Power Sources 195 (2010) 5057.
[23] L.J. Wang, X.C. Zhou, Y.L. Guo, J. Power Sources 195 (2010) 2844.
[24] L. Wang, X.Q. Jiang, X. Li, X.Q. Pi, Y. Ren, F. Wu, Electrochim. Acta 55 (2010) 5057.
[25] X.H. Rui, Y. Jin, X.Y. Feng, L.C. Zhang, C.H. Chen, J. Power Sources 196 (2011) 2109.
[26] X.H. Rui, N. Yesibolati, C.H. Chen, J. Power Sources 196 (2011) 2279.
[27] Y.N. Ko, H.Y. Koo, J.H. Kim, J.H. Yi, Y.C. Kang, J.-H. Lee, J. Power Sources (2011),doi:10.1016/j.jpowsour.2010.11.086.
[28] Y.-G. Guo, J.-S. Hu, L.-J. Wan, Adv. Mater. 20 (2008) 2878.
[29] F. Yu, J.J. Zhang, Y.F. Yang, G.Z. Song, J. Power Sources 195 (2010) 6873.
[30] F. Yu, J.J. Zhang, Y.F. Yang, G.Z. Song, J. Mater. Chem. 19 (2009) 9121.
[31] J.Z. Chen, L. Yang, Y.F. Tang, J. Power Sources 195 (2010) 6893.
[32] X.H. Huang, J.P. Tu, B. Zhang, C.Q. Zhang, Y. Li, Y.F. Yuan, H.M. Wu, J. Power Sources 161 (2006) 541.
[33] S.Q. Wang, J.Y. Zhang, C.H. Chen, J. Power Sources 195 (2010) 5379.
[34] X.Y. Han, Q.F. Meng, T.L. Sun, J.T. Sun, J. Power Sources 195 (2010) 3047.
[35] X.H. Huang, J.P. Tu, C.Q. Zhang, X.T. Chen, Y.F. Yuan, H.M. Wu, Electrochim. Acta 52 (2007) 4177.
[36] H.-M. Xie, R.-S. Wang, J.-R. Ying, L.-Y. Zhang, A.F. Jalbout, H.-Y. Yu, G.-L. Yang, X.-M. Pan, Z.-M. Su, Adv. Mater. 18 (2006) 2609.
[37] H.M. Wu, J.P. Tu, Y.Z. Yang, D.Q. Shi, J. Mater. Sci. 41 (2006) 4247.
[38] F. Yu, J.J. Zhang, Y.F. Yang, G.Z. Song, J. Power Sources 189 (2009) 794.
[39] B. Huang, X.D. Zheng, D.M. Jia, M. Lu, Electrochim. Acta 55 (2010) 1227.
[40] X.Y. Wang, S.Y. Yin, K.L. Zhang, Y.X. Zhang, J. Alloys Compd. 486 (2009) L5.
[41] C.M. Burba, R. Frech, Solid State Ionics 177 (2007) 3445.
[42] J.Y. Xiang, X.L. Wang, X.H. Xia, L. Zhang, Y. Zhou, S.J. Shi, J.P. Tu, Electrochim. Acta 55 (2010) 4921.
[43] J.Y. Xiang, J.P. Tu, L. Zhang, X.L. Wang, Y. Zhou, Y.Q. Qiao, Y. Lu, J. Power Sources 195 (2010) 8331.
[44] K. Dokko, M. Mohamedi, M. Umeda, I. Uchida, J. Electrochem. Soc. 150 (2003) A425.
[45] J. Xie, N. Imanishi, T. Zhang, A. Hirano, Y. Takeda, O. Yamamoto, J. Power Sources 189 (2009) 365.
[46] Y.H. Rho, K. Dokko, K. Kanamura, J. Power Sources 157 (2006) 471.